TiO_2-SiO_2-Reinforced Methylated Grafted Natural Rubber (MG49-TiO_2-SiO_2) Polymer Nanocomposites: Preparation, Optimization and Characterization

Oon Lee Kang[1, 4], Azizan Ahmad[1]*, Nur Hasyareeda Hassan[1]*, Usman Ali Rana[2], Mohd Sukor Suait[3], and Claudio Migliaresi[4]

[1]Faculty Science and Technology, Universiti Kebangsaan Malaysia, 43600 Bangi, Selangor, Malaysia
[2]Sustainable Energy Technology Center, King Saud University, P.O. Box 800, Riyadh 11421, Saudi Arabia
[3]Solar Energy Research Institute, Universiti Kebangsaan Malaysia, 43600 Bangi, Selangor, Malaysia
[4]Biotech Research Center, Universita di Trento, via delle Regole 101, 38123 Mattarello, Trento, Italy

SUMMARY

TiO_2-SiO_2 (30:70) and (70:30) sol particles were first prepared through $ClHNO_2$-EtOH catalysis; and then incorporated into methylated grafted natural rubber (MG49) polymer host. Resultant MG49-TiO_2-SiO_2 (30:70) and (70:30) polymer nanocomposites were characterized through XRD and FTIR analyses. Both MG49-TiO_2-SiO_2 (30:70) and (70:30) polymer nanocomposites had exhibited extensive reduction in semicrystalline phase; but no significant change in structural properties. Low crystalline MG49-TiO_2-SiO_2 (30:70) and (70:30) polymer nanocomposites were further characterized through SEM, TGA and DRA analyses. Both MG49-TiO_2-SiO_2 (30:70) and (70:30) polymer nanocomposites had exhibited different dispersion state on fracture surface. Both MG49-TiO_2-SiO_2 (30:70) and (70:30) polymer nanocomposites had demonstrated significant improvement in thermal properties, and also some improvement in rheological properties.

Keywords: TiO_2-SiO_2 nanoparticle, MG49 polymer host, MG49-TiO_2-SiO_2 polymer nanocomposite

1. INTRODUCTION

Particle-reinforced natural rubber polymer nanocomposites have attracted considerable attention in fundamental research[1,2]. Indeed, particle-reinforced natural rubber polymer nanocomposites could offer considerable potential in several different fields[3]. Particle-reinforced natural rubber polymer nanocomposites have attained impressive improvement in some operational performances[4]. Particle-reinforced natural rubber polymer nanocomposites can accommodate extreme deformation over broad operational conditions. Nonetheless, there are still some limitations on current operational applications.

Recent research efforts have focused attention on concrete operational improvements. Particle dispersion behavior is important determinant in critical operational performances[5]. Different dispersion behavior can cause unpredictable effects in several operational properties (e.g. rheological, mechanical and thermal properties)[6,7]. Uniform dispersion state is fundamental prerequisite to superior operational performance[8]. Such preference attribute is more related to percolation network formation. Second preference attribute is often attributed to tremendous interfacial interaction. However, particle dispersion mechanism is still not understood in detail[9].

Particle-reinforced natural rubber polymer nanocomposites are often obtained through nanoparticle reinforcement. However, there are still some limitations in this approach[9]. In the present research, TiO_2-SiO_2-reinforced methylated grafted natural rubber (MG49-TiO_2-SiO_2) polymer nanocomposites were prepared through sol-gel nanoparticle formation. Resultant polymer nanocomposites were characterized through several different instrumental techniques.

2. MATERIALS AND METHOD

2.1 TiO_2-SiO_2 Sol Particle Preparation

TiO_2-SiO_2 (30:70) and (70:30) sol particles were prepared through $ClHNO_2$-EtOH catalysis. TiO_2-SiO_2 sol solutions were obtained at four different predetermined molar ratios (**Table 1**). TiO_2-SiO_2 sol solutions

*Corresponding author: syareeda@ukm.edu.my; azizan@ukm.my

Table 1. Hydrolysis molar ratio

Metal alkoxide $[Si_4(OCH_2CH_3)_{16}$: $Ti_4(OCH_2CH_3)_{16}]$	Catalyst $[ClHNO_2]$	Solvent [Ethanol]	H_2O
1	1	4	4
1	1	4	8
1	1	4	16
1	1	4	32

were stirred ½ hours at ambient room temperature. Resulted sol particles were dried and stored until analysis.

2.2 MG49-TiO_2-SiO_2 Polymer Nanocomposite Preparation

MG49-TiO_2-SiO_2 polymer nanocomposites were obtained through solution-cast techniques. TiO_2-SiO_2 sol particles (R_w = 16) were introduced into preformed MG49 polymer matrices. Resultant mixtures were stirred ½ hours at ambient temperature. Homogeneous mixtures were cast into a Teflon petri dish. Resultant films were further dried in vacuum oven.

2.3 MG49-TiO_2-SiO_2 Polymer Nanocomposite Characterization

DLS analyses were conducted on a Malvern Zetasizer Nano ZS DLS spectrometer (Malvern Instruments Ltd., United Kingdom). DLS analyses were performed at a fixed detection angle (θ = 173°). DLS data were acquired in the backscatter mode. DLS data were analyzed through the Zetasizer software.

XRD analyses were conducted on a Bruker D8 Advance diffractometer (Bruker AXS, Germany). XRD analyses were performed at the CuKα radiation wavelength (λ=0.154 nm). XRD patterns were acquired in the Bragg-Brentano configuration. XRD patterns were recorded in the 2θ range (15-60°; step size 0.02°).

FTIR analyses were conducted on a Perkin-Elmer Spectrum 400 FTIR spectrometer (Perkin Elmer, UK). FTIR spectra were acquired in Attenuated Total Reflectance (ATR) mode. FTIR spectra were recorded in the mid infrared range (4000-650 cm^{-1}; spectral resolution 4 cm^{-1}).

SEM analyses were conducted on a LEO 1450 VP instrument (Carl Zeiss AG, Oberkochen, Germany). SEM analyses were performed at a low acceleration voltage (~5 kV). SEM micrographs were acquired in the secondary electron (SE) mode. SEM micrographs were taken at a high magnification.

TGA analyses were conducted on a Shimadzu TGA-50 instrument (Shimadzu, Japan). TGA thermograms were recorded in a broad temperature range (30-600 °C; scan rate 10 °C·min^{-1}).

DRA analyses were conducted on Anton Paar Physica MCR 501 rheometer (Anton Paar, Austria). DRA analyses were performed in the linear viscoelastic region. DRA responses were acquired in a dynamic oscillation mode.

3. RESULTS AND DISCUSSION

3.1 TiO_2-SiO_2 Nanoparticle Characterization

Monodisperse particle size distribution was observed at different hydrolysis ratio. In this case, narrowest particle size distribution was observed at moderate hydrolysis ratio (R_w=16). Smallest particle size (≤100 nm) is prone to agglomerate formation. Such phenomenon can cause unpredictable effects on performance properties.

Non-crystalline (amorphous) TiO_2-SiO_2 structure was observed at low hydrolysis ratios ($R_w \leq 16$). Meanwhile, semicrystalline TiO_2-SiO_2 structure was observed at high hydrolysis ratio (R_w=32). Semicrystalline TiO_2-SiO_2 structure is attributed to Si suppressive effect. Three dominant bands were observed in the TiO_2-SiO_2 spectra

Figure 1. Size distribution profiles (a) TiO_2-SiO_2 (30:70) nanoparticle and (b) TiO_2-SiO_2 (70:30) nanoparticle

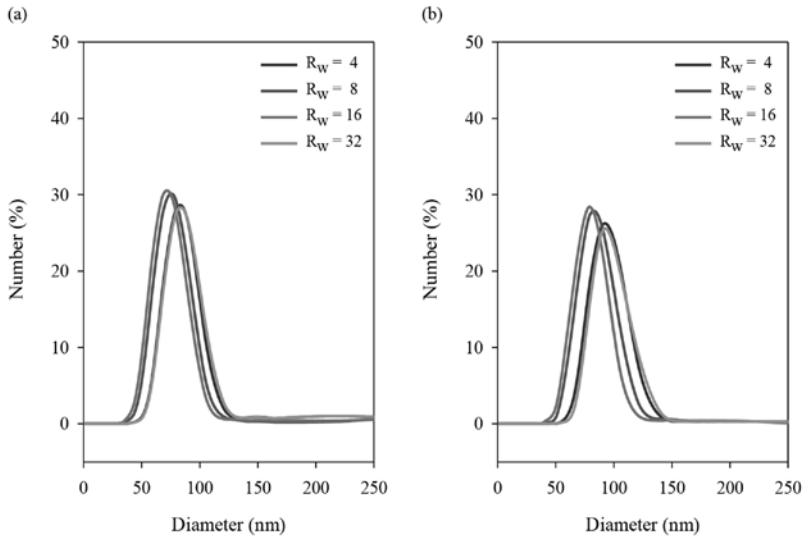

(**Figure 3**). Ti-O-Ti absorption band was observed at 810 cm^{-1}. Si-O-Ti absorption band was observed at 940 cm^{-1}. Si-O-Si absorption band was observed at 1060 cm^{-1}.

3.2 MG49-TiO_2-SiO_2 Polymer Nanocomposite Characterization

Three characteristic diffraction peaks were observed in the MG49 diffraction profile. Such characteristic diffraction peaks are attributed to isoprene/methyl methacrylate monomer. Preferable characteristic diffraction peak (2θ = 15°) had become flattened upon TiO_2-SiO_2 reinforcement. Such phenomenon is attributed to amorphization. In addition, such characteristic diffraction peak (2θ = 15°) had distorted upon TiO_2-SiO_2 reinforcement. Such phenomenon is attributed to lattice distortion. TiO_2-SiO_2 diffraction peaks were not observed in the MG49-TiO_2-SiO_2 (30:70) and (70:30) diffraction pattern. Such phenomenon is attributed to particle-polymer compatibility.

IR absorption spectrum is comparable to earlier reports. Carbonyl ν(C=O) absorption band was observed at 1725 cm^{-1}. Meanwhile, ester (C–O-C) absorption band was observed around 1250-950 cm^{-1}. Both absorption bands did not shift upon TiO_2-SiO_2 reinforcement. In such a case, interfacial interaction is attributed to percolation network formation, rather than covalent interaction.

Morphological surface structure was characterized prior to rheological and thermal analysis. Smooth surface feature was observed in the MG49 polymer host. Smooth surface feature is attributed to brittle fracture behavior. Meanwhile, rough surface feature was observed in the MG49-TiO_2-SiO_2 (30:70) and (70:30) polymer nanocomposites. Rough surface feature is attributed to particle-polymer interaction.

Particle dispersion behavior is quite different in the MG49-TiO_2-SiO_2 (30:70) and (70:30) polymer nanocomposites. Particle agglomeration process had occurred in the MG49-TiO_2-SiO_2 (30:70) and (70:30) polymer nanocomposites.

Figure 2. XRD diffraction patterns (a) TiO_2-SiO_2 (30:70) nanoparticle and (b) TiO_2-SiO_2 (70:30) nanoparticle

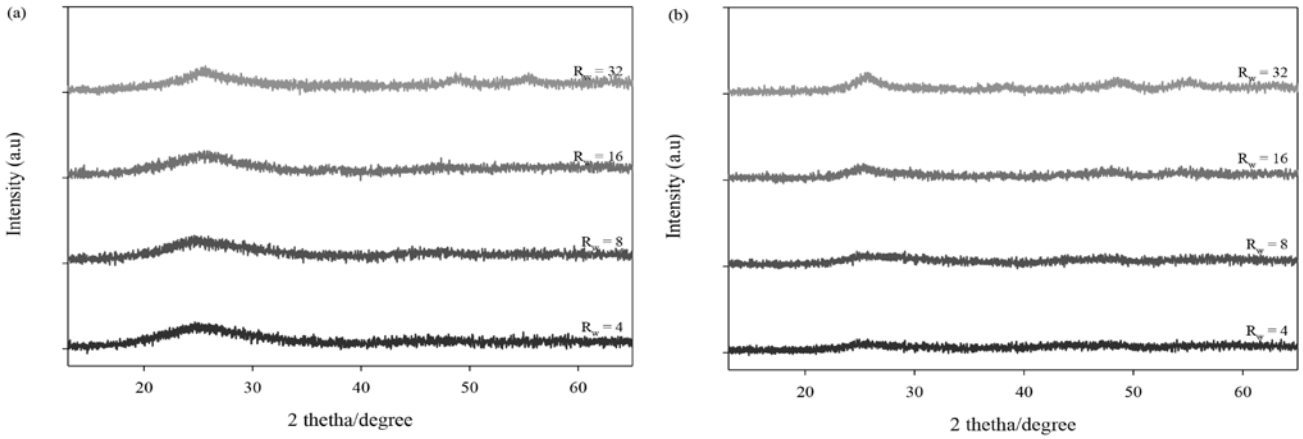

Figure 3. FTIR transmittance spectra (a) TiO_2-SiO_2 (30:70) nanoparticle and (b) TiO_2-SiO_2 (70:30) nanoparticle

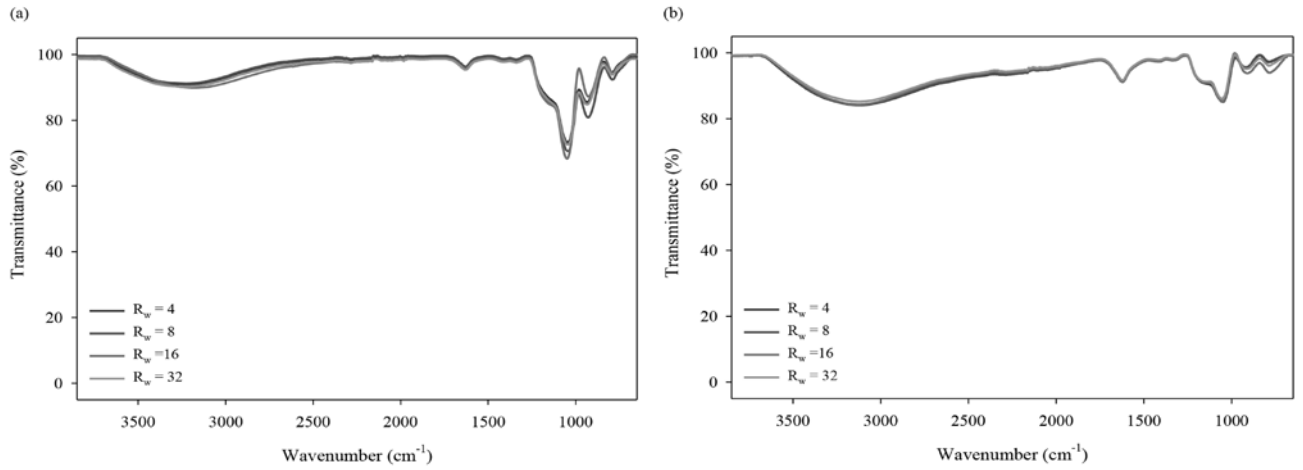

Figure 4. X-ray diffraction patterns (a) MG-49-TiO_2-SiO_2 (30:70) polymer nanocomposite and (b) MG-49-TiO_2-SiO_2 (70:30) polymer nanocomposite

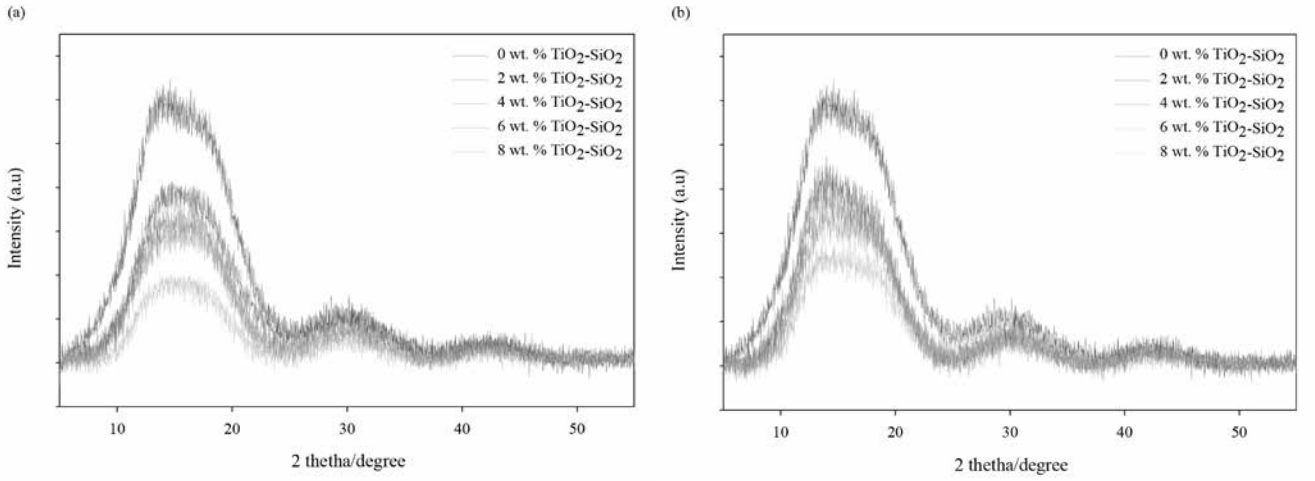

Figure 5. FTIR transmittance spectra (a) MG-49-TiO_2-SiO_2 (30:70) polymer nanocomposite and (b) MG-49-TiO_2-SiO_2 (70:30) polymer nanocomposite

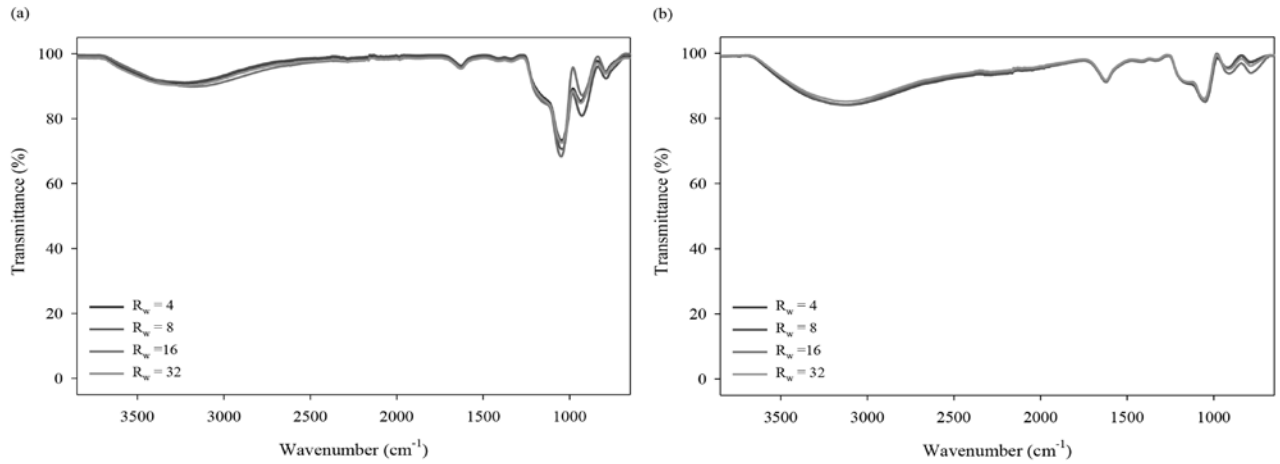

In the present case, particle agglomeration effect is more pronounced in the MG49-TiO_2-SiO_2 (30:70) polymer nanocomposite. Unavoidable agglomeration process is attributed to small particle size, i.e. large surface area and high surface energies[10].

Individual degradation process was observed in MG49 polymer host. Thermal degradation temperature was observed around 300-450 °C, as indicated in the DTA signal. Such degradation process is attributed to oxidative decomposition. Thermal degradation process is initiated through random chain scission. Similar degradation pattern was observed in the MG49-TiO_2-SiO_2 (30:70) and (70:30) polymer nanocomposites. Such phenomenon is attributed to particle-polymer compatibility. In this case, however, minor weight loss is detected at low temperature range. Such phenomenon is attributed to TiO_2-SiO_2 catalytic effects. Onset degradation temperature had shifted towards high temperature range. Such phenomenon is attributed to stability improvement. Thermal degradation process is suppressed upon particle-polymer interaction[11]. However, intrinsic degradation mechanism is still not understood in detail.

G' and G" modulus had remained constant over small strain change; and then G′ and G″ modulus had decreased above critical strain amplitude. Such phenomenon is attributed to network breakdown[12]. In effect, high deformation rate had resulted in poor mechanical properties. Linear viscoelastic range had become narrowed upon TiO_2-SiO_2 reinforcement. Such phenomenon is attributed to particle-particle interaction. G′/G″ crossover point had shifted upward upon TiO_2-SiO_2 reinforcement. Phase structure transition is hindered upon particle-polymer interaction. G′ modulus had increased upon TiO_2-SiO_2 reinforcement. Polymer chain relaxation is restrained upon particle-polymer interaction[6]. However, polymer chain motion is not affected upon particle-polymer interaction.

Figure 6. SEM-EDX micrograph (a) MG49 polymer host, (b) MG49-TiO_2-SiO_2 (30:70) polymer nanocomposite and (c) MG49-TiO_2-SiO_2 (70:30) polymer nanocomposite

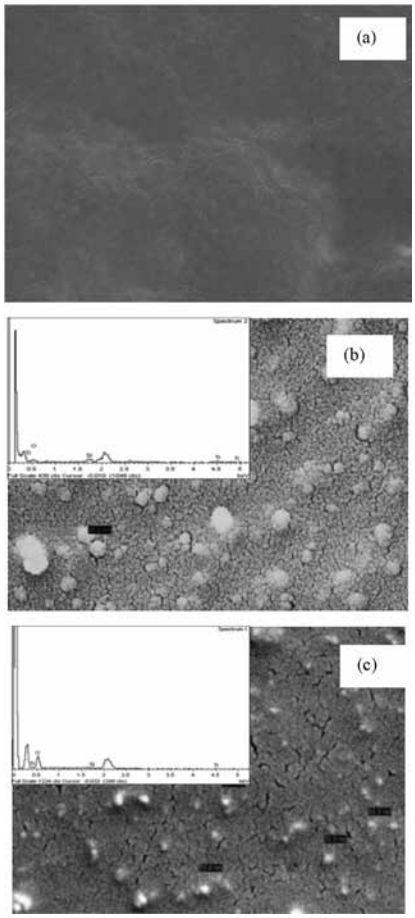

Figure 7. TGA curves (a) MG49 polymer host, (b) MG49-TiO_2-SiO_2 (30:70) polymer nanocomposite and (c) MG49-TiO_2-SiO_2 (70:30) polymer nanocomposite

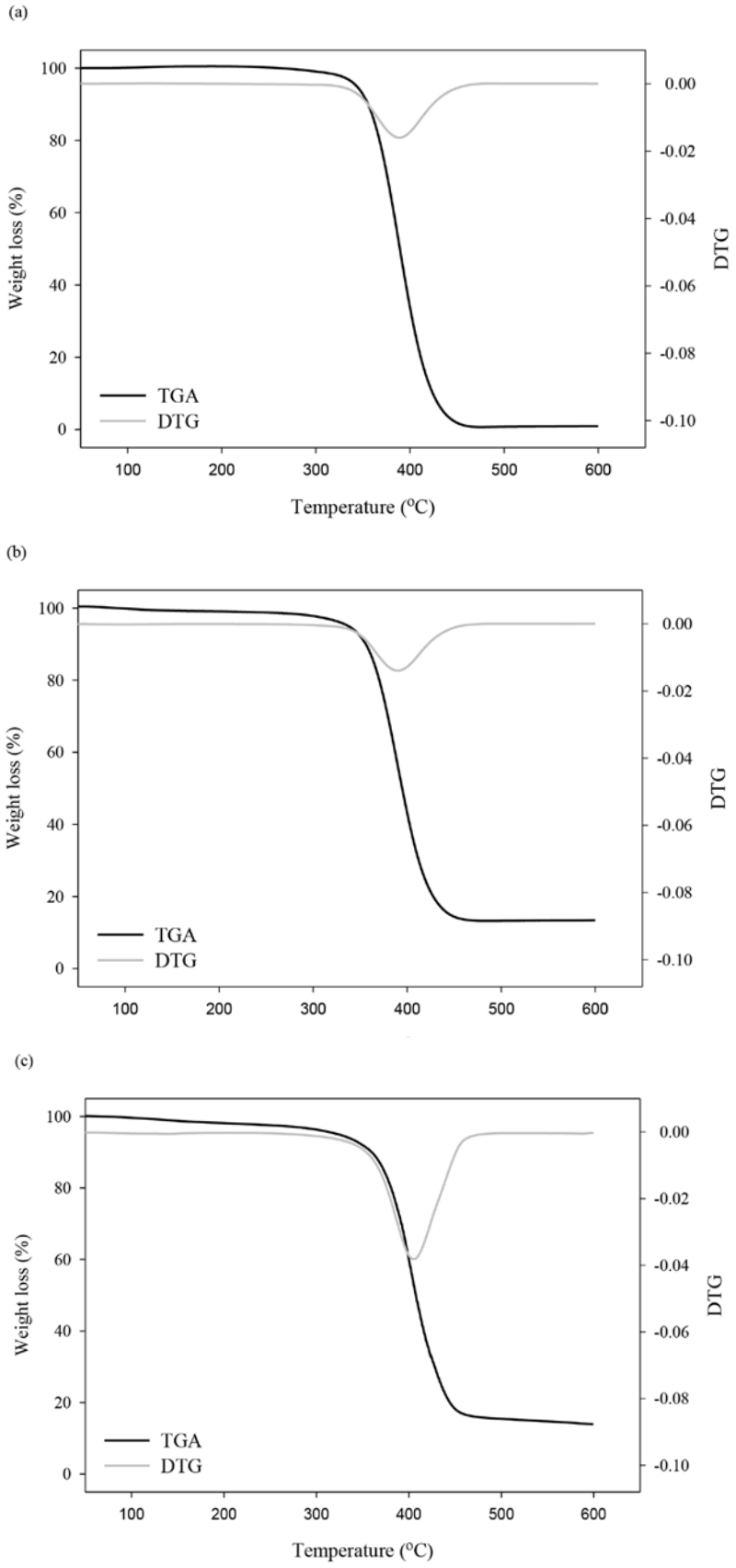

G′ and G″ modulus had remained constant throughout the entire frequency range. Such phenomenon is attributed to predominant elastic properties. 1,4-polyisoprene soft segment structure could contribute to elastic properties. G′ > G″ is attributed to high storage stabilities. Plateau modulus had become more apparent upon TiO_2-SiO_2 reinforcement. Such phenomenon is attributed to percolation network formation[13]. G′ modulus had reduced upon TiO_2-SiO_2 reinforcement. Such phenomenon is attributed to physical crosslink density reduction.

Figure 8. Strain sweep curve (a) MG49 polymer host, (b) MG49-TiO_2-SiO_2 (30:70) polymer nanocomposite and (c) MG49-TiO_2-SiO_2 (70:30) polymer nanocomposite

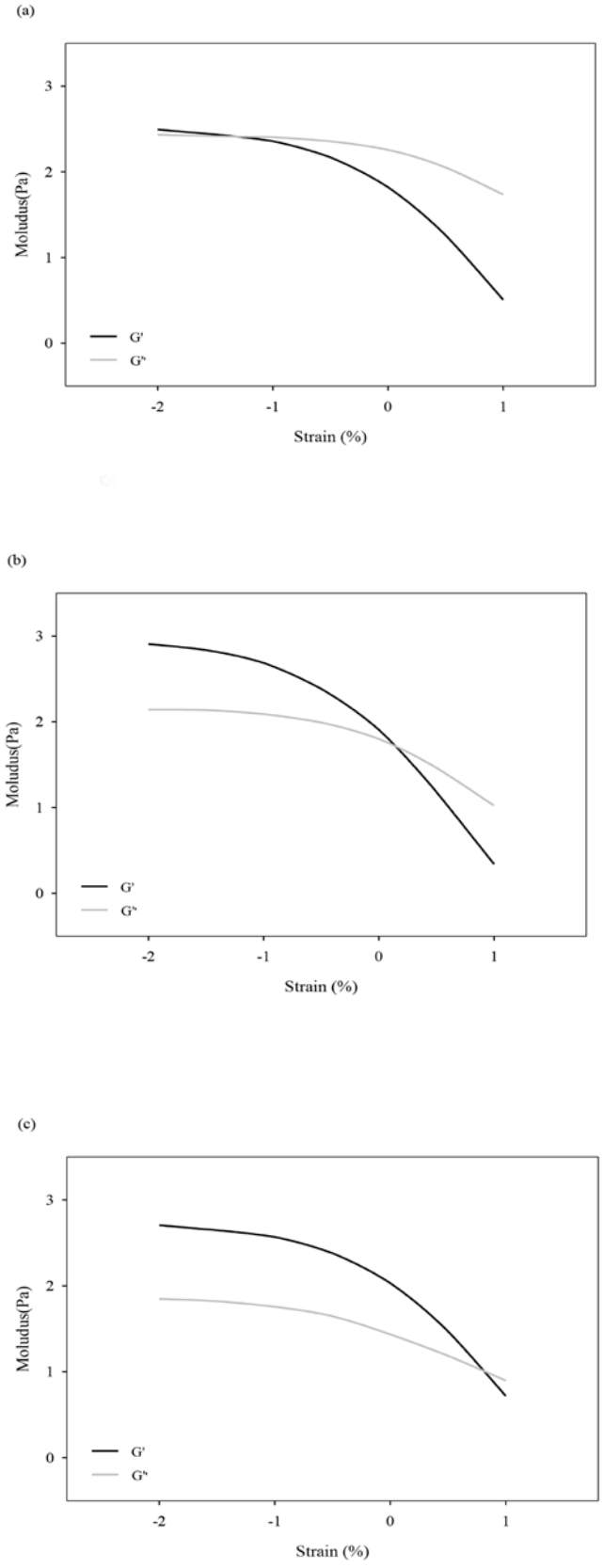

Figure 9. Frequency sweep curve (a) MG49 polymer host, (b) MG49-TiO_2-SiO_2 (30:70) polymer nanocomposite and (c) MG49-TiO_2-SiO_2 (70:30) polymer nanocomposite

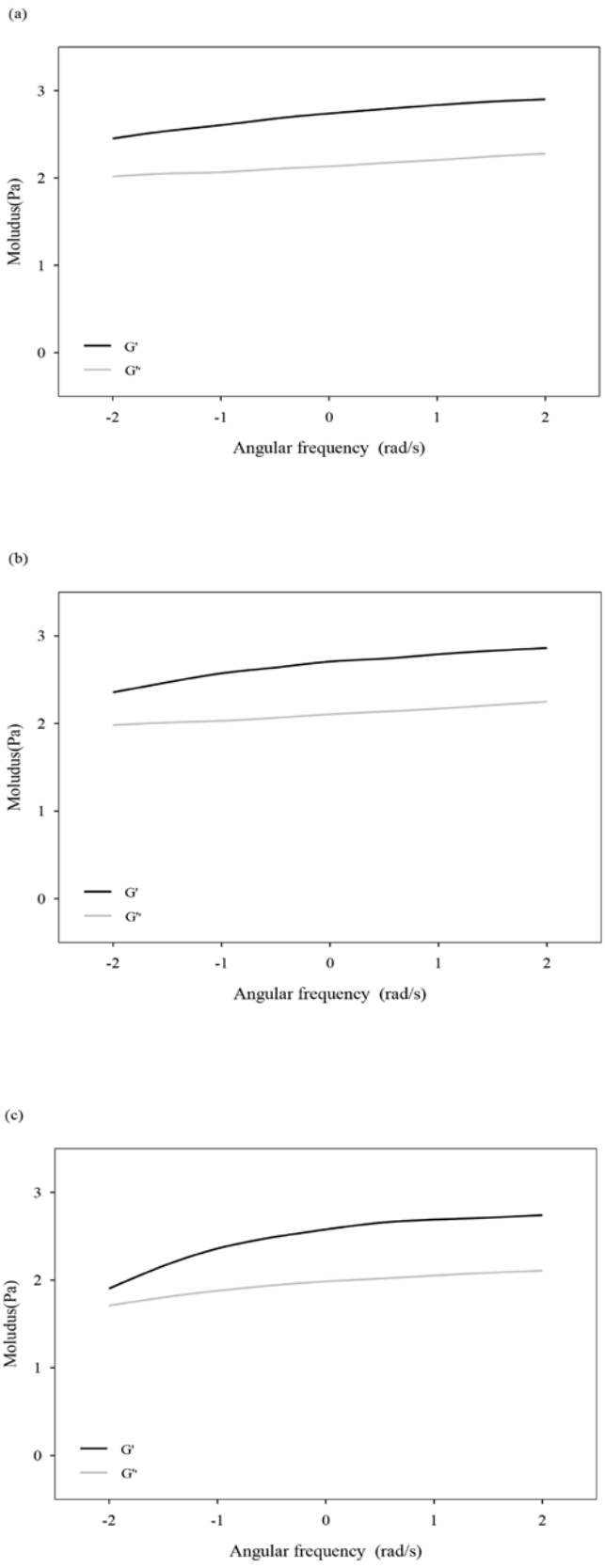

4. CONCLUSIONS

MG49-TiO_2-SiO_2 (30:70) and (70:30) polymer nanocomposite had exhibited *different characteristics than* MG49 polymer host. In particular, resultant polymer nanocomposites had achieved *better* predictive stabilities than MG49 polymer host. In such a case, MG49-TiO_2-SiO_2 (30:70) and (70:30) polymer nanocomposites can offer great opportunities in *numerous technological applications*.

ACKNOWLEDGEMENT

Authors would like to acknowledge financial support from research grant: (1) NND/NM (2)/TD11-046 and (2) ERGS/1/2013/TK07/UKM/02/4. Authors would also like to acknowledge instrumental/*technical support from CRIM*.

REFERENCES

1. Sengloyluan K., Sahakaro K., Dierkes W.K., Noordermeer J.W.M., *Eur. Polym. J.*, **51** (2014) 69-79.
2. Glasse M.D., Idris R., Latham R.J., Linford R.G., Schlindwein W.S., *Solid State Ionics*, **147** (2002) 289-294.
3. Manaila E., Stelescu M.D., Doroftei F., *Iran Polym. J.*, **24** (2015) 135-148.
4. Poochai C., Paeon P., Pongpayoon T., *World Acad. Sci. Eng. Technol.*, **4** (2010) 756-760.
5. Motovilin, M., Denchev, Z., Dencheva, N., *J. Appl. Ploym. Sci.*, **120** (2011) 3304-3315.
6. Man Y.H., Li Z.C., Zhang Z.J., *Mater. Trans.*, **50** (2009) 1355-1359.
7. Potts J.R., Dreyer D.R., Bielawski C.W. Ruoff R.S., *Polymer*, **52** (2011) 5-25.
8. Zou H., Wu S. Shen J., *Chem. Rev.*, **108** (2008) 3893-3957.
9. Eitan A., Fisher F.T., Andrews R., Brinson L.C., Schadler L.S., *Compos. Sci. Technol.*, **66** (2006) 1159-1170.
10. Peponi L., Tercjak A., Martin L., Mondragon I., Kenny J.M., *Express Polym. Lett.*, **5** (2011) 104-118.
11. Juby K.A., Charu D.C., Kumar M., Kota S., Misra H.S. Bajaj P.N., *Carbohydr. Polym.*, **89** (2015) 906-913.
12. McCann J., Behrendt J.M., Yan J. Halacheva S., Saunders B.R., *J. Colloid Interface Sci.*, **449** (2015) 21-30.
13. Kota A.K., Cipriano B.H., Duesterberg M.K., Gershon A.L., Powell D., Srinivasa R., Raghavan S.R., Bruck H.A., *Macromolecules*, **40** (2007) 7400-7406.